Chem Soc Rev

Cite this: *Chem. Soc. Rev.*, 2012, **41**, 8050–8065

www.rsc.org/csr

TUTORIAL REVIEW

Shape control of bimetallic nanocatalysts through well-designed colloidal chemistry approaches†

Jun Gu,[a] Ya-Wen Zhang*[a] and Franklin (Feng) Tao*[b]

Received 22nd May 2012
DOI: 10.1039/c2cs35184f

Synthesis of bimetallic nanomaterials with well controlled shape is an important topic in heterogeneous catalysis, low-temperature fuel cell technology, and many other fields. Compared with monometallic counterparts, bimetallic nanocatalysts endow scientists with more opportunities to optimize the catalytic performance by modulating the charge transfer between different metals, local coordination environment, lattice strain and surface element distribution. Considering the current challenges in shape controlled synthesis of bimetallic nanocatalysts, this tutorial review highlights some significant achievements in preparing bimetallic alloy, core–shell and heterostructure nanocrystals with well-defined morphologies, summarizes four general routes and some key factors of the bimetallic shape control scenarios, and provides some general ideas on how to design synthetic strategies to control the shape and exposing facets of bimetallic nanocrystals. The composition and shape dependent catalytic behaviours of bimetallic nanocrystals are reviewed as well.

[a] *Beijing National Laboratory for Molecular Science, State Key Laboratory of Rare Earth Materials Chemistry and Applications, PKU-HKU Joint Laboratory in Rare Earth Materials and Bioinorganic Chemistry, College of Chemistry and Molecular Engineering, Peking University, Beijing 100871, China. E-mail: ywzhang@pku.edu.cn; Fax: +86 10 62756787; Tel: +86 10 62756787*
[b] *Department of Chemistry and Biochemistry, University of Notre Dame, Notre Dame, IN 46556, USA. E-mail: ftao@nd.edu; Tel: +1 574 631 1394*
† Part of the bimetallic nanocatalysts themed issue.

1. Introduction

Noble metal catalysts are widely used in the fields of energy conversion and storage, environmental remediation, chemical production, *etc*. Improving the catalytic performance (activity, selectivity and durability) and minimizing the usage of noble metals have remained as the major tasks in numerous investigations for decades.[1] Bimetallic nanocatalysts provide a promising path towards this goal and attract tremendous attention from

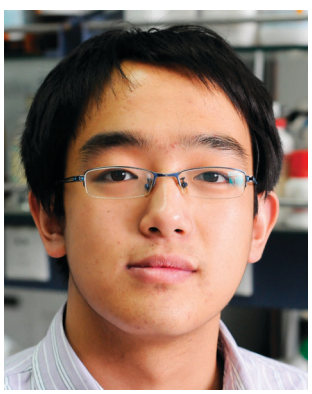

Jun Gu

Jun Gu was born in December of 1988 in Shanxi of China. He received his BSc degree in Chemistry from Peking University in 2011. Now he is working for his PhD degree under the supervision of Prof. Yawen Zhang in College of Chemistry and Molecular Engineering, Peking University. His current research focuses on the colloidal synthesis and catalytic property investigation of noble metal based nanomaterials.

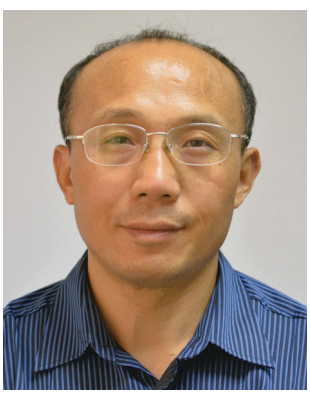

Ya-Wen Zhang

Yawen Zhang is full professor and principle investigator at College of Chemistry and Molecular Engineering of Peking University. The research interests of his group are focused on the rational design, controllable synthesis, ordered assembly, catalytic properties and structure–function relationships of rare earth and noble metal nanostructures. He has published more than 100 papers in peer-reviewed scientific journals and was a Winner of National Science Fund for Distinguished Young Scholars in 2010. He obtained his BSc degree, MSc degree, and PhD degree from Peking University in 1988, 1994 and 1997, respectively, and did postdoctoral research in State Key Laboratory of Rare Earth Materials Chemistry and Applications of Peking University during 1998–2000, and has been a visiting scholar in Department of Chemistry of University of California at Berkeley and Lawrence Berkeley National Laboratory during 2006–2008.

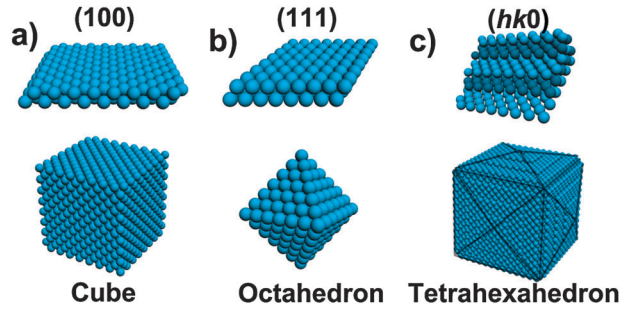

Fig. 1 Schematic of some examples of atomic arrangement on the surface of face centred cubic (fcc) metal crystals with different shapes. (a) Cube exposes {100} facets. (b) Octahedron exposes {111} facets. (c) Tetrahexahedron exposes {hk0} facets containing atomic steps and terraces.

chemists and material scientists. Alloying a parent metal with a second metal offers numerous opportunities for tuning electronic states of the catalysts and optimizing their catalytic properties.

As shown in Fig. 1, metal crystals with different shapes expose different facets (*hkl*) which typically have different atomic arrangements in their surface layers. These different facets have distinct surface electronic and geometric structures, leading to the variation in adsorption energy of reactants or intermediates in heterogeneous catalysis.[1,2] Therefore, shape control is critical for both monometallic and bimetallic nanocrystals (NCs). El-Sayed's group first realized the shape selective synthesis of metal NCs, obtaining Pt nanocubes and nanotetrahedrons exposing {100} and {111} facets, respectively.[3] Somorjai's group demonstrated the shape-dependent catalytic selectivity in benzene hydrogenation on Pt nanocubes and nanocuboctahedrons.[2]

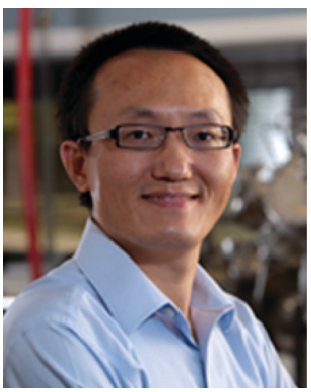

Franklin (Feng) Tao

Franklin (Feng) Tao joined Department of Chemistry and Biochemistry at University of Notre Dame as a tenure-track assistant professor in 2010 after obtaining a PhD in chemistry from Princeton University followed by a post-doctoral fellowship at Lawrence Berkeley National Laboratory and University of California at Berkeley. He is currently leading a research group interested in catalysis, energy science, and nanoscience. His group synthesizes nanocatalysts and performs operando and in situ studies of catalysis in energy conversion, chemical transformation, and environmental remediation by using operando and in-situ techniques including in-house ambient pressure XPS and ambient pressure high temperatures STM available in his group and other synchrotron-based techniques through collaborations. He has published more than 70 peer-reviewed research articles in international journals and two books by Wiley. He serves on the editorial boards or advisory editorial boards of a few journals including Chemical Society Reviews, Catalysis Science and Technology, and Scientific Reports (NPG).

Different metal surfaces constructed from heteroatoms offer multiple catalytic sites with different binding configurations for a reactant molecule or intermediate, which could potentially vary the catalytic performance significantly. One example is that the Pd–Au (100) surface prepared by deposition of Pd on Au(100) offered a proper site distribution for coupling adsorption of ethylene and acetone species, and vinyl acetate could form on the Pd–Au (100) surface.[4] Furthermore, catalytic performances of bimetallic NCs are also strongly correlated with lattice strain, which can be rationally modulated through the control over the nanostructures of the NCs. For instance, the lattice mismatch between the core and shell regions of PtCu@Pt nanoparticles can arouse the lattice strain in the Pt shell and thus enhance the activity of oxygen reduction reaction (ORR).[5]

The colloidal chemistry approach is one of the most powerful methods to prepare metallic NCs with well-defined shapes.[6] The size and shape of mono-metallic NCs can be well controlled by the careful selection of metal precursors, reductants, capping agents, solvents, temperature, reaction time, *etc*. The shape control of bimetallic NCs can be further modulated by several variables of the two constituting metals, including the reduction potential, relative decomposition/reduction rate of precursors and interfacial energy. Through different synthesis routes, researchers have prepared bimetallic core–shell, heterostructure and alloy NCs with various morphologies such as polyhedrons (single-crystalline[7–11] and multi-twinned[12]), nanorods[13] and nanowires,[14,15] nanodendrites,[16,17] multi-pods,[18,19] hollow structure,[20,21] concave structure,[22,23] *etc*. These synthetic routes can be categorized into four types: (1) continuous growth, (2) crystallites coalescence, (3) seeded growth, and (4) galvanic replacement reaction, as illustrated in Fig. 2. This article is organized by first explaining general principles underlying these four general synthetic routes and introducing some key factors of the shape control of bimetallic NCs, then illustrating by using real synthesis cases how to design a rational synthetic strategy according to the target bimetallic nanostructures, followed by reviewing some examples of bimetallic NCs that demonstrate shape correlated structure sensitivities in some important catalytic reactions, and ending with a vision of the challenges we face and the prospect in this field.

2. General principles underlying four shape control routes to bimetallic NCs

In this section, we will first give a brief introduction to four general shape-control routes in bimetallic NCs synthesis. Then we will summarize the roles of some key factors in these routes.

2.1 Four basic routes to bimetallic NCs

Generally speaking, the formation of a metallic nanocrystal (NC) can be divided into two steps: nucleation and growth. In the former two routes, the precursors of different metals are mixed together at the very beginning and the two steps of the nanocrystal growth are carried out in a one-pot reaction. Nuclei form first in these two routes. In the first route (Fig. 2a), metal atoms or clusters reduced from precursors

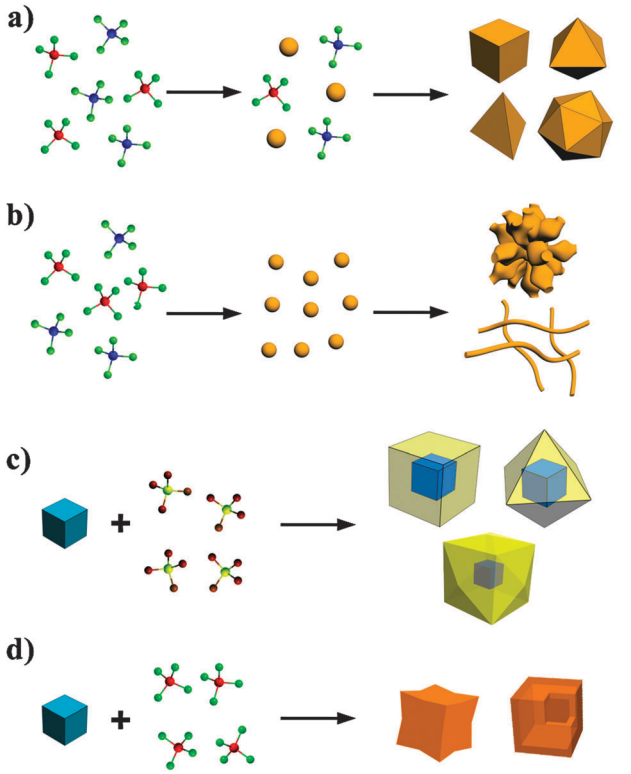

Fig. 2 Four routes towards shape-controlled bimetallic NCs: (a) continuous growth, (b) crystallites coalescence, (c) seeded growth and (d) galvanic replacement reaction. Blue, red and yellow parts stand for mono-metal and orange parts stand for alloy.

are added to these nuclei continuously, and the nuclei grow big into uniform alloy NCs. We define it as the continuous growth route. In the second route (Fig. 2b), these nuclei are directed to coalesce into one dimensional or dendritic nanostructure during the growth stage. Thus, we defined it as the crystallites coalescence route. In the latter two routes, initial metal seeds are needed. In the seeded growth route (Fig. 2c), the metal salt is reduced by a reductant in solution, and the second metal grows on the surfaces of the initial seeds. As a result, core–shell or heterostructure bimetallic NCs are produced from this route. In the galvanic replacement reaction route (Fig. 2d), the metal salt of second metal is reduced by sacrificial metal seeds. The dissolution of seeded metal and the deposition of growing metal take place simultaneously on one NC. In this case, concave or hollow alloy NCs are created. It is noteworthy that some real synthetic strategies involve two or more of these four basic routes at the same time.

In the continuous growth route, both nucleation and growth steps should be carefully controlled. In the nucleation stage, the rapid reduction rate will lead to single-crystalline nuclei and the slow reduction rate favors the formation of five-fold twinned nuclei. The former ones can serve as the seeds of polyhedrons that show O_h and T_d symmetry such as cubes, octahedrons and tetrahedrons.[7,8,10,11] The latter ones can serve as the seeds of polyhedrons that show I_h symmetry, such as icosahedrons and dodecahedrons.[12] To obtain bimetallic NCs with well-defined shape, the growth step must be guided by some facet specific capping agents, such as small molecules with selective adsorption capability on a specific facet. If a set of facets are strongly capped by capping agents, growth on these facets will be hindered.[7,8,10,11] When some oxidants such as O_2 coexist with halide ions in the solution, the oxidative etching of bimetallic NCs will occur simultaneously in the growth stage. This process can also be guided by facet-specific capping agents and can be used to synthesize concave and multipod structures.[19]

In the crystallites coalescence route, growth and coalescence of metal nuclei are two competing processes. A high reduction rate is needed for this route, which leads to explosive nucleation and favors the formation of numerous tiny crystallites with high surface energy. Unlike the continuous growth route, in this route, most monomers are consumed in the nucleation stage and few monomers are left for every individual crystallite to grow. These crystallites tend to aggregate to decrease their total surface energy. After the attachment of bimetallic crystallites, metal atoms around the interface of two crystallites will diffuse across the interface and finally several crystallites will fuse into one NC. In the continuous growth route, the shape evolution of the bimetallic NCs is mainly determined by the growth rate on different facets, which can be controlled by using facet-specific capping agents. In this route, to obtain bimetallic NCs with specific morphology, one should control the way these crystallites attach to each other. For instance, polymer-formed micelles can serve as templates in the coalescence process, and porous dendritic structure can be obtained. Facet-specific capping agents can vary the energy barrier for coalescence on different facets and guide the facet-oriented coalescence process, which leads to the formation of bimetallic nanowires.[14,15]

In the seeded growth route, the structure of produced NCs is firstly dependent on the growth mode of the second metal growing on the seeds. Generally, there are three types of growth mode near equilibrium states, the layered growth (Frank–van der Merwe mode, F–M mode), the island growth (Volmer–Weber mode, V–W mode), and the intermediate mode (Stanski–Krastanow mode, S–K mode).[24] Small lattice mismatch and a strong bond between seed and shell atoms favor the F–M growth mode, and an intact epitaxial shell can form on a given seed. Otherwise, the growth step of second metal will follow the V–W mode, and core–shell NCs with rough, polycrystalline shells or binary structure NCs will form.[25] A rapid reduction rate will break the near equilibrium condition and favors the island growth. Secondly, just like the case of the continuous growth route, the growth stage of second metal in this route is also guided by facet-specific capping agents.[9]

In the galvanic replacement reaction route, initial seeds are also needed, but the precursor of second metal is reduced by the core metal instead of reductants in solution. It is needed that the redox potential of the second metal must be higher than that of the seeded metal. Cations of the second metal first adsorbed on the surface of a seed. The cations get electrons from the seed and the positive charge moves away from the deposition sites. Simultaneously, some seeded metal atoms on the surface lose electrons and diffuse into solution. The deposition and dissolution sites are strongly dependent on the surface capping agents. In this route, facet-specific capping

agents can be used to direct the formation of many complex bimetallic nanostructures such as concave cubes and multipod structures.[18]

2.2 Key factors in four routes

Four basic routes towards shape-controlled bimetallic NCs have been concisely described in the last subsection. In practice, many intrinsic and extrinsic factors determine by which route a synthetic reaction will take place, and how the shape of bimetallic NCs evolves in every route. Herein, we summarize five important factors that govern the shapes of bimetallic NCs in the above four routes: (1) redox potentials of different metals, (2) interfacial energy, (3) reduction rates of metal precursors, (4) facet-specific capping agent effects and (5) temperature and reaction time. In this subsection, we will discuss how we can control these factors by choosing chemical reagents (such as capping and reducing agents) and tuning experimental conditions, and how these factors affect the shape evolution in four routes. Then we can rationally design the synthetic strategies according to our demand.

2.2.1 Redox potentials of different metals. Standard reduction potential (SRP) is always used to quantify the difficulty in reducing a metal precursor. The more positive the SRP is, the easier the metal precursor can be reduced. Although SRP is defined in aqueous solution, it still shows a trend of reducibility of different metal precursors in non-aqueous solution. SRP of different metals can be tuned in a range by changing the ligands that coordinate with the metal ions, as shown below:

$$\varphi^{\circ}([ML_x]^{n-mx}/M) = \varphi^{\circ}(M^{n+}/M) - \frac{0.059}{n}\log K \qquad (1)$$

In this equation, cation M^{n+} can coordinate with ligand L^{m-} to form the complex $[ML_x]^{n-mx}$. $\varphi^{\circ}(M^{n+}/M)$ is the SRP of free cation M^{n+} and $\varphi^{\circ}([ML_x]^{n-mx}/M)$ is the SRP of the complex $[ML_x]^{n-mx}$. K is the stability constant of $[ML_x]^{n-mx}$. The tighter L^{m-} species coordinate with M^{n+} ions, the more positive constant K is. From this equation, we can conclude that using ligands that strongly coordinate with the metal cations can lower the redox potential of the metal cations and make the reduction of the metal cations more difficult. These ligands can be incorporated in the metal precursors, or be added separately into the solution. Halide ions have strong affinity towards noble metal ions and can lower the redox potential of these metals.

When strongly bound ligands are used to decrease the redox potential of center ions, the reduction rate of the metal precursor will be decreased and the reaction will be under near equilibrium conditions. These ligands often serve as capping agents that strongly cap a certain set of facets at the same time. Under this condition, the growth rate on the facets that are strongly capped will be lower, and these facets will be retained in the final product.[26] The growth of a certain facet here refers to the addition of newly reduced metal atoms above this facet, so the growth direction is perpendicular to this facet. If the reduction potential of the precursor is comparatively high, the reduction process will be fast. In this situation, facets with high surface energy are more likely to be exposed and thermodynamically unfavoured structures can be obtained. More detailed effects of the reduction rate will be discussed in Section 2.2.3.

If the reducing process is in the near equilibrium state, a metal precursor with high redox potential will be reduced preferentially to the other metal precursor. The SRPs of noble metals are much higher than those of non-noble metals. If our goal is to synthesize alloy NCs containing noble metals and non-noble metals through the continuous growth route, we need to decrease the redox potential difference between two metal precursors. We can use ligands to coordinate strongly with the noble metal ions to lower their redox potential. And at the same time, an interesting phenomenon called underpotential deposition (UPD) facilitates the reduction of non-noble metal ions on the noble metal surfaces. UPD is a phenomenon by which the electro-deposition of metal monolayers on a foreign metal substrate can be performed at potentials significantly less negative than that for deposition on the same metal surface as a adsorbate.[27] As a result, the existing noble metal nuclei can induce the reduction of non-noble metal ions. Based on the UPD phenomenon, Li and co-workers synthesized a series of noble-metal-based alloy NCs in octadecylamine.[28] As long as the effective electronegativity of the alloy is higher than 1.93, the corresponding alloy NCs can be obtained by this method. Besides the redox potential difference of two metal precursors, the heat of mixing of two different metals also determines whether alloy or monometallic NCs will be obtained. The more negative the heat of mixing is, the more possible alloy NCs will form. For instance, the values of heat of mixing of Pt–Ni and Pt–Cu are quite negative while those of Pt–Au or Pt–Ag are quite positive.[29] As a consequence, Pt–Ni alloy NCs could form even though an Ni(II) precursor was added after the formation of Pt NCs,[8] while some alloy NCs such as Au–Pt alloy NCs are more difficult to prepare.

In the presence of oxidants such as O_2, as-reduced metal atoms can be oxidized back to metal ions, as is called the oxidative etching process. Halide ions, which strongly coordinate with noble metal ions, can suppress the reduction of noble metal ions, and in return, facilitate the oxidation of these metals. For example, Pd atoms on the surface of a Pd-based NC can be oxidized by the Br^{-}–O_2 pair:

$$Pd + 1/2O_2 + 4Br^{-} + 2H^{+} \rightarrow PdBr_4^{2-} + H_2O \qquad (2)$$

The redox potential difference is also the driving force for the galvanic replacement reaction. The redox potential of the second metal should be considerably higher than that of the core metal. Ligands that facilitate the oxidation of the core metal are indispensable in many cases. For instance, Br^{-} ions are often used as the oxidation facilitator of Pd. The galvanic replacement reaction between Pd seeds and Pt^{2+} ions can take place only in the presence of Br^{-} ions.[18] If no Br^{-} ions were introduced, the reaction would follow the seeded growth route instead of the galvanic replacement reaction route in the presence of weak reductants such as citric acid, and Pd@Pt NCs will form.[30]

2.2.2 Interfacial energy. The thermodynamic stability of bimetallic core–shell NCs is mainly determined by the interfacial energy between two metals. Low interfacial energy

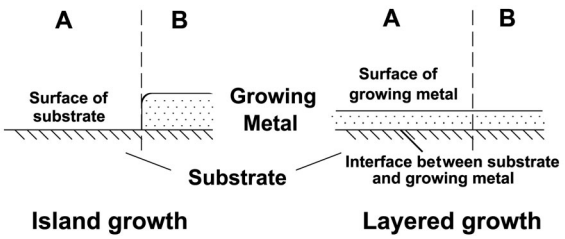

Fig. 3 Schemes of island growth model and layered growth model.

favors the layered growth of the shell metal and high interfacial energy leads to island growth.[24,25] As shown in Fig. 3, the left model stands for island growth and the right model stands for layered growth. In the island growth model, the growing metal is located in Region B, and in Region A the substrate metal is exposed. In the layered growth model, both Region A and Region B are covered by growing metal. We define γ_{s-g}, γ_s and γ_g as the interfacial free energy per unit area between substrate and growing metals, surface free energy per unit area of substrate metal and growing metal, respectively. S stands for the area of Region A. Therefore, the free energy difference between the layered growth model and the island growth model is:

$$G_{\text{layered growth model}} - G_{\text{island growth model}} = S(\gamma_{s-g} + \gamma_g) - S\gamma_s \quad (3)$$

If layered growth is thermodynamically favored, it is demanded that:

$$\gamma_{s-g} < \gamma_s - \gamma_g \quad (4)$$

Eqn (4) shows that $\gamma_s - \gamma_g$ is a critical value. If the interfacial energy is below this value, layered growth is favored. If the interfacial energy is above this value, island growth is favored.

Two main factors determine the interfacial energy. One is the lattice match between two sets of metal lattices, and the other one is the bond between atoms in the overlayer and the substrate.[25] Large lattice mismatch leads to large lattice strain and raise the interfacial energy. We define n as the number of growing layers. The lattice strain and the interfacial energy γ_{s-g} increase with n. If eqn (4) can be fulfilled for all n, the F–M mode layered growth will be obtained. If eqn (4) breaks down at a critical n^*, the layered growth is confined within a few layers (S–K mode). If eqn (4) cannot be fulfilled at $n = 1$, V–W mode island growth will be obtained.[24]

When we introduce above growth models into core–shell NCs, we should consider the effects of nanoscale dimensions. The tolerance of lattice mismatch on the nanoscale is not very harsh. Au@Ag[31] and Pt@Pd[9] core–shell NCs were prepared in some early works of Yang and co-workers. The lattice mismatch of Au–Ag and Pt–Pd is very small, *i.e.* 0.25% and 0.77% respectively. Tian and co-workers first realized the preparation of Au@Pd core–shell NCs despite the lattice mismatch being 4.88%.[25] Though the lattice mismatch of Au–Pt (4.08%) is smaller than that of Au–Pd, Au@Pt core–shell NCs with intact single-crystalline shells still cannot be synthesized. They proposed the following rules for the epitaxial layered growth of core–shell NCs: lattice mismatch between two sets of lattices should be smaller than 5% and the bond between atoms in the overlayer and the substrate should be stronger than the bond between two atoms in the overlayer.[25] In a very recent work of Xia and co-workers, Cu could still be epitaxially deposited on Pd seeds to form Pd@Cu core–shell nanocubes in hexadecylamine, despite the lattice mismatch between Cu and Pd being 7.1%.[32] This result may be due to the strong affinity between Pd and Cu. Another driving force is the decrease of the surface energy of NCs. Hexadecylamine can stabilize the surface of Cu and decrease the surface free energy of Cu (γ_g), which facilitates epitaxial seeded growth, as shown in eqn (4).

If the growth of the second metal on a single-crystalline seed follows the layered growth mode, an intact single-crystalline shell with the same lattice orientation as the seed will form. The shape of core–shell bimetallic NCs can be controlled by using facet-specific capping agents. If the growth of the second metal follows the island growth mode, binary structure NCs are often obtained.[9] Core–shell NCs can still be obtained at fast growth rates, but the shells are often polycrystalline due to the lack of an epitaxial relationship between the core and the shell. Then the shape of final products is often spherical[25] or dendritic,[31] and cannot be controlled by facet-specific capping agents.

2.2.3 Reduction rate. The reduction rate of metal precursors is affected by many factors, including the redox potential of precursors, the reducing capacity of a reductant, reaction temperatures, *etc*. $NaBH_4$ and hydrazine are widely used as reductants in the synthesis of metal NCs, while their strong reducibility leads to a too fast reduction and the shape of products is often difficult to control. To realize shape control, many milder reductants have been exploited. In an organic solvent system, amine[7,10] and polyol[22] often serve as reductants and solvents at the same time. In an aqueous phase system, ascorbic acid (AA)[9,16] and formaldehyde[11,12] are often used. Capping agents such as citric acid[30] and poly(vinylpyrrolidone) (PVP) with terminal hydroxyl groups can also serve as weak reductants.[11,23] The reduction rate of a certain reductant can be tuned by changing its concentration. In aqueous phase synthesis, it can also be modulated by adjusting the pH value. Here we can take formaldehyde as an example. The formaldehyde oxidation half-reaction is shown as:

$$HCHO + H_2O \rightarrow 4H^+ + CO_2\uparrow + 4e^- \quad (5)$$

Since H^+ appears as a product in this half reaction, the reducing capacity of formaldehyde will be significantly suppressed when the pH value is low.[12]

When the reduction rate is slow, the nucleation and growth processes will be under near-equilibrium conditions, and the fast reduction rate will break down near-equilibrium conditions. As discussed in Section 2.2.1, in one-pot synthesis, the metal precursor with high redox potential will be reduced preferentially to the other precursor under near-equilibrium conditions, and the reaction will follow the seeded growth route and core–shell bimetallic NCs tend to be obtained. In contrast, the fast reduction rate favors the formation of alloy NCs.

In the nucleation stage, a low reduction rate favors the formation of multi-twinned seeds. The specific surface area of multi-twinned seeds, such as decahedrons and icosahedrons, is smaller than that of cubes and octahedrons with the same amount of atoms, and multi-twinned seeds expose only the {111} facet, whose surface free energy is the lowest among those of several low-index facets in many cases. The twinned defects in a multi-twinned seed will increase the total free energy. If the seed is very tiny, the energy cost in twinned defects can be compensated by the energy gained in total surface free energy, then a multi-twinned seed is thermodynamically favored. With a slow reduction rate, multi-twinned structures can form before metal seeds grow big. Once twinned defects form, the energy barrier for the reconstruction from a twinned crystal to a single crystal is very high. Therefore, in the continuous growth route, a low reduction rate is needed for the preparation of multi-twinned bimetallic NCs, while single-crystalline NCs form at a high reduction rate.[6]

If the reduction rate is further increased, it will lead to explosive nucleation and rapid consumption of metal precursors. The nucleation consumes most of the precursors and few precursors are left for further growth. This leads to a large amount of tiny crystallites. In order to decrease the total surface free energy, the reaction will follow the crystallites coalescence route.

In the seeded growth route, a high reduction rate will initiate multi-site growth on the surface of the given seeds and favors island growth. In a typical case, K_2PdCl_4 was reduced by AA in the presence of Pt nanocubes. The reducing capacity of AA could be modulated by adjusting the pH value of the aqueous solution. In a neutral condition, well-defined Pt@Pd core–shell NCs were obtained. In a basic environment, the reducing capacity of AA was enhanced and the reduction rate of $PdCl_4^{2-}$ was increased, leading to multi-site nucleation and the localized growth of Pd atoms on cubic Pt seeds.[33]

Fig. 4 schematically shows how the reduction rate affects the formation of bimetallic NCs when $HAuCl_4$ and K_2PtCl_4 were used as precursors. If only cetyltrimethylammonium chloride (CTAC) was used and no extra reductant was introduced, metal precursors would be reduced by CTAC very slowly and Au@Pd core–shell nanooctahedrons formed after 30 h (Fig. 4a).[34] If ascorbic acid was introduced to increase the reduction rate, Au–Pd alloy nanooctahedrons formed after 2 h (Fig. 4b).[34] If the reduction process was further accelerated by increasing the concentration of L-ascorbic acid, thermodynamically unfavored

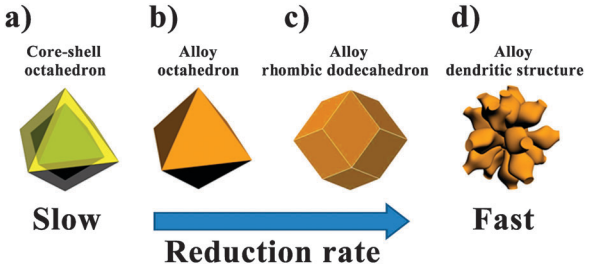

Fig. 4 Different Au–Pd bimetallic NCs obtained with different reduction rates: (a) Au@Pd core–shell octahedron, (b) Au–Pd alloy octahedron, (c) Au–Pd rhombic dodecahedron, (d) Au–Pd nano-dendrite.

Au–Pd alloy rhombic dodecahedrons enclosed by twelve {110} facets could form after 1 h (Fig. 4c).[35] If hydrazine was used as a reductant with very strong reducibility, Au–Pd alloy nano-dendrites could form within 5 min (Fig. 4d).[36] Therefore, a high reduction rate leads to simultaneous reduction of metal precursors and the formation of thermodynamically unfavored NCs.

2.2.4 Facet-specific capping agent effects. To synthesize bimetallic NCs with well-defined shape exposing specific facets, facet-specific capping agents are indispensable. These agents can be the counter ions in the precursors, solvents, salts, surfactants, polymers, gas molecules, *etc*. Table 1 lists some commonly used facet-specific capping agents. In aqueous-phase synthesis, halide ions are often used as the {100} facet-specific capping agents for most *fcc* structured bimetallics.[6,9,21] Among them, Br^- and I^- ions show better facet-selectivity than Cl^- ions. PVP is often used as the stabilizer for metallic NCs. In most cases, PVP shows poor facet-selectivity, but it is indispensable for preventing metallic NCs from aggregation. Citric acid,[30] NO_2,[9] and $C_2O_4^{2-}$[11,12] can serve as the {111} facet-specific capping agents in Pt and Pd-based bimetallics.

In an organic solvent system, organic amines and acids are commonly used as the capping agents, but their roles as facet-specific capping agents are still not very clear. Alkyl groups affect the interaction between these species and different metal facets. Wu and Yang showed that, in Pt-based alloys, when the length of the alkyl group was increased, the exposure of the {100} facets would be favored.[37] A recent work of Li and co-workers showed that benzoic acid can be used as the {111} facet-specific capping agent that inhibits the growth on the {111} facets of the Pt–Ni alloy.[38] CO, generated from the decomposition of metal carbonyl or introduced additionally, can also serve as a co-capping agent together with oleylamine (OAm).

Table 1 Commonly used facet-specific capping agents and their preferentially binding facets

Agents	Preferentially binding facets
Br^-, I^-	{100} facets of Pt, Pd, Ag, Au and their alloy[6,9,40]
NO_2	{111} facets of Pd[9]
$C_2O_4^{2-}$	{111} facets of Pt- and Pd-based alloy[11,12]
Citric acid	{111} facets of Pt and Pd and their alloy[30]
Benzoic acid	{111} facets of Pt-Ni alloy[38]
CO + OAm	{100} facets of Pt and Pt-based alloy[7,8,10]
	{111} facets of Pt based alloy[8,10]
DMF	{100} facets of Pt-Ni alloy with high Pt/Ni ratio[39]
	{111} facets of Pt-Ni alloy with low Pt/Ni ratio[39]

In most cases, Pt-based alloy nanocubes were obtained in the presence of CO and OAm,[7,37] while some recent studies showed that the role of CO strongly depends on the composition of the NCs and the solvent. Fang and co-workers showed that the combined use of OAm and CO can stabilize the {100} facets of Pt and the {111} facets of the Pt_3Ni alloy.[8] If Pt^{II} and Ni^{II} precursors were introduced together, nanooctahedrons that exposed {111} facets were obtained. If Pt^{II} and Ni^{II} precursors were introduced in sequence, Pt nanocubes would form first and then the Ni^{II} precursor would be reduced and alloy with Pt. Pt_3Ni alloy nanocubes would be obtained finally.[8] The effect of CO also alters as the solvent composition changes. In the synthesis of Pt_3M (M = Fe, Co, Ni, Pd) alloy NCs, if CO was used together with OAm and OA, nanocubes exposing {100} facets would form. If CO was used together with OAm and biphenyl ether, nanooctahedrons exposing {111} facets would form.[10] DMF, which is commonly used in solvothermal synthesis, also shows some facet-specific capping properties. In a recent work of Carpenter and co-workers, Pt–Ni alloy NCs with well-defined morphology were synthesized through a solvothermal method in DMF. If the ratio of Pt–Ni was high, the NCs tended to expose {100} facets and showed cubic morphology. If the ratio of Pt–Ni was low, the NCs tended to expose {111} facets and showed octahedral morphology.[39] This indicates that the relative binding preference of DMF on different facets alters as the composition of bimetallic NCs changes.

Many steps in bimetallic NCs synthesis are controlled by facet-specific capping agents. First of all, facet-specific capping agents can guide the growth stage in the continuous growth route and the seeded growth route. Two general effects are concerned in the growth stage. On one hand, capping agents can lower the surface energy of bimetallic NCs. If a kind of capping agent strongly binds on a set of facets, the surface energy of these facets will decrease. To obtain the lowest total surface free energy, the facets with lowest surface free energy tend to expose more in a thermodynamically favored final product. On the other hand, capping agents can decrease the growth rate on certain facets. If a kind of capping agent binds on a set of facets more tightly, the coverage of capping agents on these facets will be higher and fewer sites will be left for growth. Facets with high growth rates will diminish and disappear during the growth stage and facets with low growth rates will be retained in the end. The former effect is discussed in a thermodynamic control regime and the latter effect is discussed in a kinetic control regime. The growth stage at high temperature and a relatively low reduction rate will be under thermodynamic control and the morphology of final products depends on the relative surface energy of different facets. The growth stage at low temperature and a relatively high reduction rate will be under kinetic control and the morphology of final products depends on the relative growth rate of different facets.[26] But, in general, the trends of these two effects are similar: facets that are bound more tightly by capping agents tend to be retained. If {100} facet-specific capping agents are used, cubes are more likely to be obtained. If {111} facet-specific capping agents are used, octahedrons, tetrahedrons and icosahedrons are more likely to form.

Dissolution of surface atoms of bimetallic NCs is also affected by capping agents. In the oxidative etching process, halide ions can assist O_2 to dissolve the surface atoms. Since halide ions, especially Br^- ions, strongly bind on {100} facets, the concentration of halide ions around {100} facets is significantly higher than that around other facets. Consequently, the oxidative etching process will take place mainly along six ⟨100⟩ directions.

Galvanic replacement reaction involves growth and dissolution at the same time, so it is also affected by facet-specific capping agents. In a recent work of Xia and co-workers, the galvanic replacement reaction between Pd nanocubes and $PtCl_6^{2-}$ was used to prepare Pt–Pd heterostructure NCs in the presence of Br^- ions.[18] Since Br^- ions facilitated the dissolution of surface atoms on {100} facets, and the eight corners of nanocubes were more accessible for Pt^{II} monomers, the oxidation half-reaction preferentially occurred on six {100} facets and the reduction half-reaction preferentially occurred at eight corners. As a result, the {100} facets of Pd nanocubes shrunk gradually and Pt atoms deposited on eight corners. When the {100} facets of Pd totally disappeared, there were no proper sites for Br^- adsorption. Then the galvanic replacement reaction was shutdown and Pd–Pt octapods were obtained finally.[18]

The general idea about the synthesis of bimetallic NCs with concave or multipod structure is facet-specific growth or dissolution. If a set of facets are strongly bound by a kind of capping agent, atoms on these facets are preferentially dissolved and growing atoms preferentially deposit on other facets.

2.2.5 Temperature and reaction time. In the above several subsections, we discussed how to control the shape evolution in four routes through the choice of precursors, reductants and capping agents. Some other external parameters, especially temperature and reaction time, are also very important.

First, high temperature will increase the decomposition and reduction rate of metal precursors. If the metal precursors are difficult to be reduced or the reducibility of reductants is weak, especially in the synthesis of bimetallic NCs containing non-noble metals, high temperature is needed to keep a reasonable reduction rate. A higher reduction rate during the nucleation stage will result in high population of nuclei. Consequently, the size of final products often decreases when reaction temperature is increased.

More importantly, the growth and coalescence regime (kinetically or thermodynamically) can be tuned by changing reaction temperature. At high temperature, the growth and coalescence tend to be isotropic, and the NCs are more likely to reach the thermodynamically stable states. Alloy NCs with the lowest surface energy, usually spheres or convex polyhedrons, are obtained in most cases. At low temperature, the reconstruction of bimetallic NCs is seriously suppressed and the growth and coalescence stage will be under kinetic control. Facets bound by fewer capping agents grow faster, or oriented attachment between two crystallites will preferentially occur on these facets. Bimetallic NCs with anisotropic structure such as nanowires[14] and concave NCs, or NCs exposed high-index facets[41,42] are more likely to be obtained at low temperature.

Temperature control is of particular importance in bimetallic nanowires synthesis through the coalescence route. At low temperature, two crystallites cannot fuse into one particle through the atomic reconstruction around the interface. At high temperature, spherical alloy NCs will form through the random aggregation of bimetallic crystallites. In a recent work of Li and co-workers, Au–Ag alloy ultrathin nanowires could be prepared in octadecylamine only at a low temperature of 90 °C.[14]

The reaction time should be determined to match the decomposition and reduction rates of the precursors. Different reaction time corresponds to different stages in the formation of bimetallic NCs. In general NC synthesis, at the beginning of the reaction, the concentration of monomers increases rapidly beyond the saturation concentration but no nuclei form. As the concentration reaches the nucleation concentration, nuclei form immediately and the monomer concentration decreases below the nucleation concentration. Then the reaction enters the growth stage.[43] At the initial stage of growth, bimetallic NCs often show poorly-defined shapes. As the reaction time increases, the NCs tend to evolve into a regular shape exposing well-defined facets with the guidance of facet-specific capping agents. Further increase of reaction time may lead to reconstruction of bimetallic NCs and Ostwald ripening process: small NCs are dissolved and large NCs grow larger. Etching of the bimetallic NCs[19] and galvanic replacement reaction[21] often accompany the growth process. In general, thermodynamically favored products are more likely to be obtained after long reaction time.

3. Shape control examples of bimetallic NCs with well-designed synthetic routes

Table 2 summarizes some of bimetallic NCs with well-defined shapes synthesized by the four routes, and lists the geometric structure of the bimetallic NCs, the route adopted, and the key factors of shape control. Based on the general principles discussed in the above sections, in this section we will use some cases in these four routes to show how to choose the reaction route, how to design synthesis strategies according to your target bimetallic nanostructures, and what should be paid special attention to in the synthesis process.

3.1 Continuous growth

Alloy nanopolyhedrons exposing well-defined facets can be prepared through the continuous growth route. Facet-specific capping agents are indispensable for modulating the surface energies and growth rates of different facets. Capping agents that strongly bind on {100} facets are needed to get alloy nanocubes and those that strongly bind on {111} facets are needed for the synthesis of alloy nanotetrahedrons or nanooctahedrons. For example, Zhang and co-workers demonstrated that Pt–Pd nanocubes can be prepared by using a mixture of Br^- and I^- ions to stabilize {100} facets (Fig. 5a), while nanotetrahedrons can be prepared by using $C_2O_4^{2-}$ ions to stabilize {111} facets (Fig. 5b).[11] Furthermore, if multi-twinned structure is our aim, the reduction rate should be decreased. Icosahedrons and dodecahedrons are enclosed by the {111} facets, therefore capping agents that strongly bind on the {111} facets should be used. In the preparation of Pd–Pt alloy icosahedrons (Fig. 5c), $C_2O_4^{2-}$ is used as the {111} facets stabilizer. To lower the reduction rate, the concentration of reductant (HCHO) was decreased, and HCl was introduced to lower the pH value according to eqn (5).[12]

Many surfactants can form reverse-micelle-like self-organized structures in organic solvent. These structures can confine the growth stage of bimetallic NCs. Alloy nanorods can be prepared by utilizing these soft templates. In a pioneering work of Sun and co-workers, FePt alloy nanorods with a diameter of about 2–3 nm were prepared in OAm.[13] The packing density of OAm was high around the rod-shaped templates and low at two ends. Thus, the surfaces of two ends of the NCs were more accessible for Fe and Pt monomers, which promote the nuclei to grow along the long axes of rods.

To prepare alloy NCs concaved along certain directions or multipod NCs, we should use facet-specific capping agents to confine the oxidative etching on some certain facets. For instance, in a recent work of Han's group, Au–Pd alloy octapodal NCs were prepared through the reduction of $NaAuBr_4$ and K_2PtCl_4 (Fig. 5d).[19] Au–Pt alloy nanooctahedrons formed first. Then Br^- ions generated from the reduction of $AuBr_4^-$ helped the oxidative etching on {100} facets. Consequently, the Au–Pt alloy nanooctahedra evolved into {100} facet-concaved truncated octahedra after 20 min and octapods after 4 h. It was essential that Br^- ions were generated gradually during the reduction process. If NaBr was introduced into the system at the very beginning, Au–Pt alloy nanooctahedrons would not form at the early stage due to the strong capping capacity of Br^- ions on the {100} facets.

3.2 Crystallites coalescence

Crystallites coalescence is an effective route to prepare bimetallic dendritic nanostructures and nanowires. Rapid reduction of metallic precursors is needed to generate numerous tiny crystallites in the nucleation stage. These crystallites serve as building blocks to build the target structures.

Owing to the porous structure of the nanodendrites, the specific surface area of these bimetallic NCs is much higher than their counterparts with similar sizes. Block copolymers containing hydrophobic groups and hydrophilic groups can cap the tiny crystallites and serve as templates for these porous structures.

Wang and Yamauchi found that the Pluronic F127 block copolymer is an efficient capping agent and template to form Pt based alloy[45] and core–shell[17] dendritic structures. The hydrophobic poly(propylene oxide) (PPO) groups have proper affinity towards Pt and Pt–Pd alloy crystallites and the crown-ether-like poly(ethylene oxide) (PEO) groups can form cavities and serve as templates for the nanoporous structures. A proper concentration of the block copolymer is a key factor for the formation of the template. If the concentration was too low, these copolymers are inadequate to guide the numerous crystallites to form porous structure. If the concentration of the block copolymer was higher than the critical micelle concentration, micelles would form and PPO groups would be hidden in the core of micelles and lose the ability to cap

Table 2 Summary of bimetallic NCs that have been successfully synthesized through routes of continuous growth, crystallites coalescence, seeded growth and galvanic replacement reaction, including alloy, core–shell and heterostructure bimetallic NCs

	Bimetallic nanostructures	Synthetic route	Key factors in the synthetic process	Synthetic cases
Alloy	 Cube	Continuous growth	Capping agents strongly bind on {100} facets	Pt–M[7,8,10,11,40]
	 Tetrahedron Octahedron	Continuous growth	Capping agents strongly bind on {111} facets	Pt–M[8,10,11,38]
	 Icosahedron	Continuous growth	Slow reduction rate; capping agents strongly bind on {111} facets	Pt–Pd[12]
	 Rod	Continuous growth	Surfactant-formed templates	Pt–Fe[1313], Pt–Cu[44]
	 Multi-pod	Continuous growth	Facet-specific oxidative etching	Au–Pt[19]
	 Dendritic structure	Crystallites coalescence	Rapid reduction; polymer-formed templates	Pt–Pd,[45] Au–Pd[36]
	 Wires	Crystallites coalescence	Facet-oriented attachment of crystallites	Au–Ag,[14] Pt–Ag[15]
	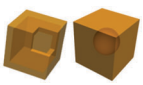 Hollow structure	Galvanic replacement reaction	Kirkendall effect	Pt–Pd[20,21]
	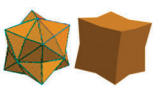 Concave structure	Galvanic replacement reaction	Underpotential deposition followed by galvanic replacement reaction	Au–Pd,[46] Pt–Cu[23]
Core–shell	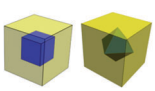 Cube	Seeded growth	Capping agents strongly bind on {100} facets	Pt@Pd,[9] Au@Pd[25,47]
	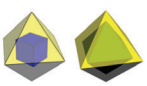 Octahedron	Seeded growth	Capping agents strongly bind on {111} facets	Pt@Pd,[9] Pd@Pt[48]
	 Core-dendritic shell	Crystallites coalescence	Rapid reduction; polymer-formed templates	Pd@Pt,[48] Pd@Rh,[49] Au@Pd@Pt[17]
	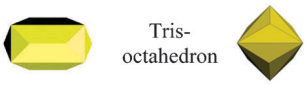 Tetrahexahedron Tris-octahedron	Seeded growth	Template-directed epitaxial deposition	Au@Pd[50,51]

Table 2 (*continued*)

Bimetallic nanostructures		Synthetic route	Key factors in the synthetic process	Synthetic cases
	Tetrahexahedron, Concave cube	Seeded growth	Large lattice mismatch; oxidative etching promoted Ostwald ripening	Au@Pd[41,42]
	Concave cube, Concave octahedron	Seeded growth	Growth rate control on different facets	Pt@Rh,[22] Au@Pd[41]
Heterostructure	Binary structure	Seeded growth	Island growth caused by large lattice mismatch or rapid reduction	Au–Pt,[9] Pt–Pd[32]
	Multi-pod	Galvanic replacement reaction	Facet-specific galvanic replacement reaction	Pd–Pt[18]

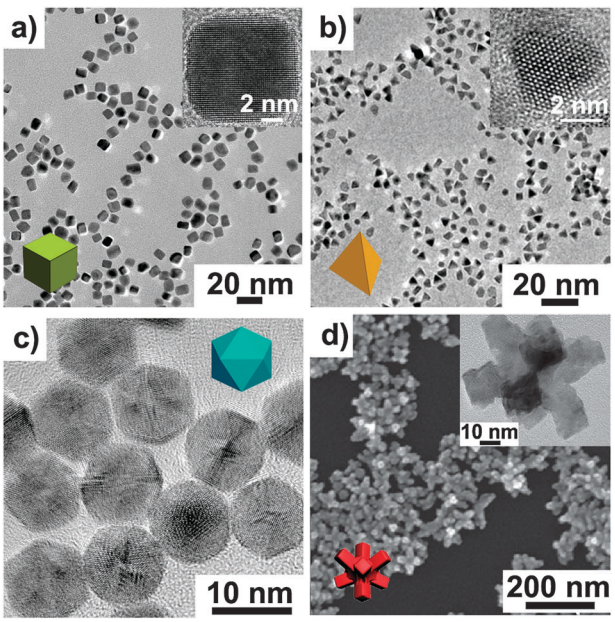

Fig. 5 Electron microscopy images of alloy NCs synthesized through the continuous growth route. (a) and (b) Transmission electron microscopy (TEM) images of Pt–Pd alloy nanocubes and nanotetrahedrons, respectively, the inset of each figure shows the corresponding high-resolution TEM (HRTEM) image (modified with permission from ref. 11, copyright 2011 American Chemical Society). (c) TEM image of Pt–Pd alloy icosahedra (modified from ref. 12). (d) Scanning electron microscopy (SEM) image of Au–Pd alloy octapodal NCs, the inset shows the TEM image of a single octapod (modified from ref. 19).

the metal crystallites. The interaction between the block copolymer and different metal surfaces varies. Since the PPO groups in the Pluronic F127 block copolymer only have a comparatively strong affinity towards Pt, it can be used to prepare Pt based dendritic structure. For instance, if $HAuCl_4$, Na_2PdCl_4 and K_2PtCl_4 were co-reduced in the presence of Pluronic F127, Au@Pd@Pt triple-layered structure with the compact Au@Pd core and the porous Pt shell would form (Fig. 6a).[17] The automatic phase separation was due to the difference in the redox potential of different precursors. Core–shell bimetallic NCs with dendritic shells can also be prepared in this route by introducing pre-synthesized seeds.[16,48] Tiny crystallites formed in the solution can coalesce on the given seeds and form porous structure under the guidance of polymeric capping agents. Generally, a high reduction rate and polymeric capping agents are indispensable for the preparation of bimetallic dendritic NCs.

Alloy nanowires can be prepared through one dimensional coalescence of alloy crystallites. In order to realize one dimensional coalescence, the direction of the coalescence process must be controlled. Thus, facet-specific capping agents are important tools to tune the coalescence energy barrier of different facets and control the coalescence direction. In a systematic work of Yang and co-workers, Pt–Ag alloy nanowires were prepared in OA/OAm mixed solvent (Fig. 6b).[15] Through density functional theory calculation, they found that the adsorption energy of OAm on {111} facets was lowest among those of three low-index facets. Therefore, the energy barrier for coalescence is lowest along the ⟨111⟩ direction. In addition, the composition of the alloy crystallites is important for the atomic diffusion across the interface of two crystallites. Molecular dynamic simulation showed that the atomic reconstruction at the interface of two particles was more kinetically favored in the $Pt_{50}Ag_{50}$ case than in other compositions.

3.3 Seeded growth

Seeded growth is the most widely used route to prepare core–shell and heterostructure bimetallic NCs. Especially, it is an effective route to prepare core–shell bimetallic NCs exposing high-index facets of the shell metal. Metallic NCs exposing high-index facets show significantly enhanced catalytic activity towards many reactions. A direct strategy is template directed epitaxial deposition. Pre-formed metallic

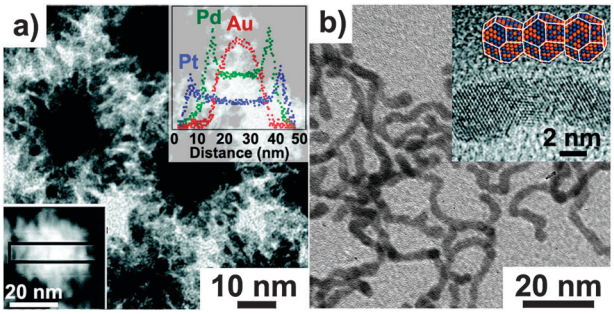

Fig. 6 TEM images of bimetallic NCs synthesized through the crystallites coalescence route: (a) Au@Pd@Pt nanodendrites, the image of high-angle annular dark-field scanning TEM (HAADF-STEM) is inserted on the left-bottom and the compositional line profiles of the area in black frame are inserted on the right-top (modified with permission from ref. 17, copyright 2010 American Chemical Society); (b) Pt–Ag nanowires, the inset shows the HRTEM of a part of a nanowire and the model shows how three pre-formed Pt-Ag crystallites coalesce into a nanowire (modified with permission from ref. 15, copyright 2010 American Chemical Society).

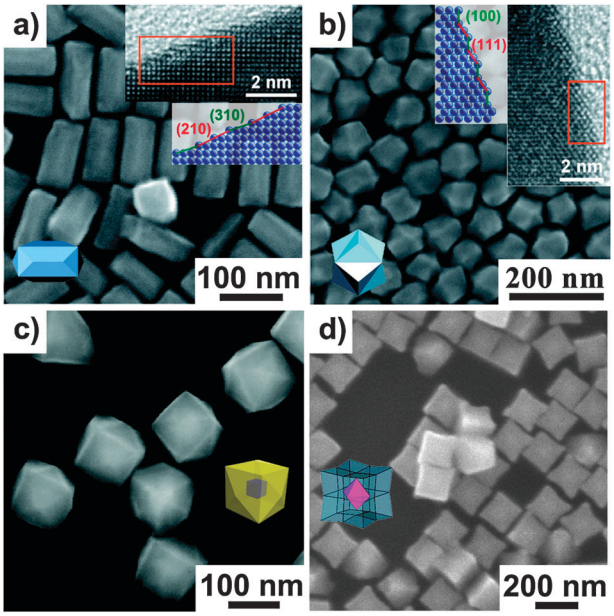

Fig. 7 SEM images of Au@Pd NCs expose high-index facets of Pd synthesized through the seeded growth route: (a) THHs and (b) TOHs with a few layers of Pd on the surface, insets show the HRTEM and schematic illustration of the surface of the two samples (modified with permission from ref. 49, copyright 2010 American Chemical Society); (c) THHs with cubic Au cores (modified with permission from ref. 40, copyright 2010 American Chemical Society); (d) concave cubes with octahedral Au cores (modified with permission from ref. 41, copyright 2011 American Chemical Society).

NCs exposing high-index facets can serve as seeds, and a few layers of shell metal atoms can be deposited on these high-index facets. Since the shells are very thin, the Miller index of the shell metal surface is the same as that of the seed surface. The method to synthesize Au NCs exposing high-index facets has been well established, but Au shows poor activity in many significant catalytic reactions. Pd can serve as a well-performed catalyst in many important reactions, so this strategy is quite useful to prepare Au@Pd core–shell NCs with Pd skin. Wang and co-workers prepared Au@Pd core–shell tetrahexahedrons (THHs) exposing {730} facets (Fig. 7a) and trisoctahedrons (TOHs) exposing {221} facets (Fig. 7b) by using this strategy.[50] Since the lattice mismatch between Au and Pd is as high as 4.88%, and only few layers of Pd atoms are deposited, the amount of Pd precursor (H_2PdCl_4) must be precisely controlled, and the reaction should be performed at room temperature to keep a slow reduction rate of the Pd precursor.

Huang and co-workers also prepared Au@Pd core–shell THH exposing {730} facets, but the formation mechanism of the high-index facets was different compared with the as-mentioned examples. Pd shells exposing high-index facets were formed on Au nanocubes which only expose {100} facets (Fig. 7c).[41] They ascribed the appearance of high-index facets of Pd to the comparatively high lattice mismatch (4.88%) at the interface of the Pd shell and the Au core. Lattice strain increased as the Pd shell grew thick. To release the high lattice strain, the high-index Pd surface unparallel to the {100} facets of Au cubic seeds formed. In addition, Cl^- ions in solution could assist O_2 to oxidize surface Pd atoms back to $PdCl_4^{2-}$. The combination of reduction and oxidation processes promoted the Ostwald ripening process of Pd and facilitated the formation of {730} high-index facets. Au@Pd concave nanocubes could be prepared through a similar strategy by introducing Au nanooctahedrons as seeds (Fig. 7d).[42]

Concave structure can also be obtained through the kinetic control of the growth rates on different facets. A relatively high reduction rate and low temperature are needed to keep the growth stage in the kinetic control regime. Facet-specific capping agents can be used to modulate the growth rate of different facets. If concave nanocubes are our target, we should choose capping agents that strongly bind on {100} facets. Thus the growth along six ⟨100⟩ directions will be significantly suppressed and the growth rate along ⟨110⟩ and ⟨111⟩ directions will be less affected. For instance, Br^- ions strongly bind on the {100} facets of Rh. Pt@Rh concave nanocubes could be prepared through the seeded growth route in the presence of Pt cubic seeds.[22] Similarly, if concave octahedrons are our target, we should choose capping agents that strongly bind on the {111} facets.

Core–shell bimetallic NCs prepared through the seeded growth route can also serve as precursors to prepare hollow structured metallic NCs. In a very recent work, Yang and co-workers prepared hollow structured NCs with various compositions through this strategy.[52] They prepared Ag@M core–shell NCs by the seeded growth route first. Then, driven by bis(*p*-sulfonatophenyl) phenylphosphane, which is strongly bound to Ag, Ag atoms in the core diffused to the surface of NC and were dissolved through oxidative etching. Ligands enhanced oxidative etching was the main driving force of this synthetic reaction.

3.4 Galvanic replacement reaction

Since galvanic replacement reaction concerns the dissolution of the sacrificial metal and the growth of the depositing metal at the same time, this route can be used to prepare bimetallic

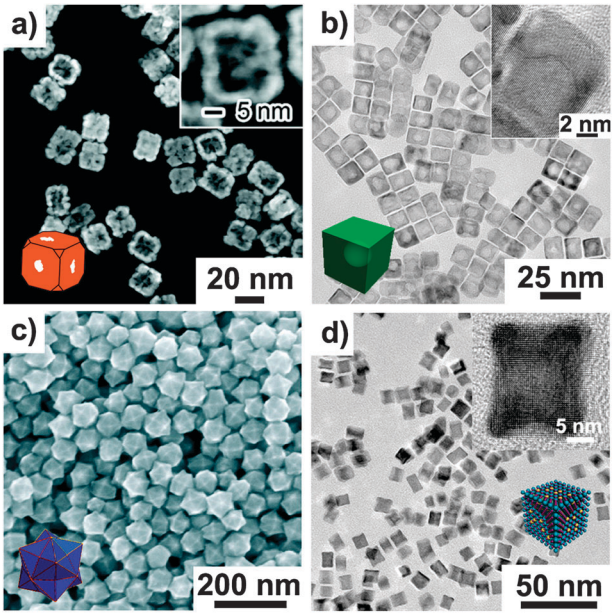

Fig. 8 Electron microscopy images of bimetallic NCs synthesized through the galvanic replacement reaction route. (a) HAADF-STEM image of Pt–Pd alloy nanocages, the inset shows an enlarged image of a single NC (modified with permission from ref. 20, copyright 2011 American Chemical Society). (b) TEM image of Pt–Pd alloy hollow nanocubes, the inset shows the HRTEM image of a single NC (modified with permission from ref. 21, copyright 2009 Wiley-VCH Verlag GmbH & Co. KGaA, Weinheim). (c) SEM image of Au–Pd alloy HOHs (modified with permission from ref. 45, copyright 2011 American Chemical Society). (d) TEM image of Pt–Cu alloy concave nanocubes, the inset shows the HRTEM image of a single NC (modified with permission from ref. 23, copyright 2012 Wiley-VCH Verlag GmbH & Co. KCaA, Weinheim).

NCs with more complex structures. Facet-specific capping agents can be used to separate the dissolution sites and deposition sites on different facets, and concave or multi-pod heterostructure NCs can be prepared, as discussed in Section 2.2.4. If an extra weak reductant is introduced in the solution, the sacrificial metal will be first oxidized by the other metal to cations, and these cations will then be reduced together with the other metal by the reductant and form alloy shells on the sacrificial seeds. Alloy nano-frameworks can be prepared through this strategy. Yang and co-workers introduced citric acid as a weak reductant into the galvanic replacement reaction between Pd cubic seeds and K_2PtCl_4, and Pt–Pd cubic alloy nano-frameworks were obtained (Fig. 8a).[20] Br^- ions are indispensable for the formation of cubic alloy nano-frameworks. On one hand, Br^- ions decreased the redox potential of Pd and promoted the galvanic replacement reaction between Pd seeds and K_2PtCl_4. On the other hand, Br^- ions stabilized the {100} facets of the Pt–Pd alloy and helped the nano-frameworks to maintain the cubic morphology.

Galvanic replacement reaction is also a practical route to prepare hollow alloy NCs. For instance, Zheng and co-workers prepared hollow Pd–Pt alloy single-crystalline nanocubes by a solvothermal method (Fig. 8b).[21] $Pd(acac)_2$, $Pt(acac)_2$ and NaI were introduced together. Since $[PdI_4]^{2-}$ is more stable than $[Pd(acac)_2]$ and $[Pt(acac)_2]$ is more stable than $[PtI_4]^{2-}$, the forms of Pd^{II} and Pt^{II} were $[PdI_4]^{2-}$ and $[Pt(acac)_2]$, respectively. The reduction of $[PdI_4]^{2-}$ was more kinetically favorable than $[Pt(acac)_2]$ under experimental conditions. Consequently, Pd nanocubes formed in the early stage although the standard reduction potential (SRP) of Pt^{II}/Pt is higher than that of Pd^{II}/Pd in the same coordination environment. Then, the galvanic replacement reaction between Pd and $[Pt(acac)_2]$ started. I^- ions here could promote the galvanic replacement reaction between Pd^0 and Pt^{II} just like Br^- ions. Thus, I^- ions served as a triple-function species in this synthesis strategy: assisting the reduction of Pd^{II}, stabilizing {100} facets of the alloy nanocubes, and promoting the galvanic replacement reaction. The hollow space in the center of Pt–Pd alloy nanocubes was a consequence of the Kirkendall effect: during the galvanic replacement reaction, Pd atoms diffused outwards and Pt atoms diffused inwards. Since the atomic radius of Pd is smaller than that of Pt, the diffusion rate of Pd atoms was much higher. As a result, hollow space formed in the center of Pt–Pd alloy nanocubes.

Underpotential deposition and galvanic replacement reaction can be combined to synthesize alloy NCs with concave structures. Proper assistant metal ions are needed in this process. In a recent work, Xie and co-workers prepared Au–Pd HOHs with the assistance of Cu^{2+} ions (Fig. 8c).[46] Since the SRP of Au^{III}/Au (1.00 V) is much higher than that of Pd^{II}/Pd (0.59 V), it is difficult to synthesize the Au–Pd alloy by direct reduction. In this Cu^{2+}-assisted reduction process, Au nuclei formed in the initial stage. The redox potential of Au/Cu (UPD) was calculated to be 0.67 V, which is just located between the SRPs of Au^{III}/Au and Pd^{II}/Pd. So Cu^{2+} ions were reduced prior to Pd^{2+} and deposited a monolayer on the Au nuclei. But the SRP of Cu^{II}/Cu (0.34 V) is lower than that of Pd^{II}/Pd, so the galvanic replacement reaction would occur after Cu deposited on Au nuclei and the Au–Pd alloy could form. A similar strategy can be used to prepare Pt–Cu and Pt–Pd–Cu alloy concave nanocubes (Fig. 8d).[23] Cu^{2+} ions were first reduced and deposited on Pt seeds due to the UPD phenomenon, and then were oxidized by Pt^{II} or Pd^{II} through galvanic replacement reaction. Br^- ions that stabilized the {100} facets of the Pt-based alloy were introduced to guide the formation of concave structure. The concentration of Pt^{II} was higher around the {100} facets of the nanocubes due to the abundant Br^- ions adsorbed on these facets. As a result, Cu atoms on the {100} facets were preferentially oxidized. The deposition of Pt and Pd preferentially occurred at the less capped eight corners of the cube, and finally Pt–Cu and Pt–Pd–Cu alloy concave nanocubes were obtained.

4. Catalytic applications of bimetallic NCs with well-controlled shape

The cost of catalysts can be reduced by partially replacing atoms of a precious metal with an earth-abundant metal. In addition, alloying a second metal offers enormous opportunities for optimizing catalytic performance of the bimetallic nanocatalysts by tuning their structural and chemical parameters. Understanding the promotion effect in catalytic behaviours and building a correlation between structural and chemical parameters of bimetallic nanocatalysts and their

catalytic performance will provide the crucial insights for rational design of robust catalysts. Plenty of investigations have been focused on the shape-sensitive catalytic performance in various reactions, especially electro-catalytic reactions involved in fuel cells. In this section, we will take oxygen reduction reaction (ORR) and methanol oxidation reaction (MOR) as examples to illustrate how morphology of bimetallic NCs affects their catalytic performances. Structural changes of shape-selective bimetallic NCs during catalytic reaction are also discussed.

4.1 Relationship between catalytic performance and the shape of bimetallic NCs

A catalytic process can be generally divided into three steps: the adsorption of reactants, reaction on the surface and the desorption of products. The relationship between catalytic activity and adsorption energy shows a volcano shape. Proper adsorption energy is needed for highest reaction activity. If the adsorption is too weak, the reactants cannot be adsorbed effectively and, thus be activated. If the adsorption is too strong, all the surface sites will be capped by intermediates and products and there will be no free sites for the adsorption of reactants. In addition, the catalytic selectivity is related to the adsorption energies of different transition states and intermediates.

Two factors have an influence on adsorption energy. One is the atomic arrangement of the surface atoms. If the atomic arrangement can match the geometry of adsorbed molecules, the distortion energy of the adsorbed molecules will be small and the adsorption will be strong. One example is the synthesis of vinyl acetate on Pd-Au bimetallic catalysts reported by Goodman's group.[4] The Pd–Au (100) surface prepared by deposition of Pd on Au(100) exhibited a much higher activity than the Pd–Au(111) surface formed on Au (111). The closest pair of Pd monomers with a distance of 4.08 Å on the Au–Pd (100) surface is favourable for the coupling of surface ethylene and acetate species in contrast to that with a large distance of 4.99 Å on the Au–Pd(111) surface. The shape of bimetallic NCs directly determines the surface atomic arrangement. The other one is electronic structure, especially the d-band center position of the surface atoms. The adsorption energy has a linear relationship with the d-band center position. The deep d-band center position leads to low adsorption energy. The d-band center position can be directly controlled by preparing alloy catalysts. For instance, the Pt–Ni alloy possesses the optimized d-band center position for ORR.[53] It can be precisely controlled by tuning the Pt–Ni ratio in the catalysts.

The shape of bimetallic NCs can also affect the d-band center position indirectly. Bimetallic NCs with different shapes expose various facets, and, thus the coordination number of surface atoms is different. A higher coordination number will lead to a deeper d-band center.[54] In addition, lattice strain caused by twinned defects[12] or the core–shell interface[5,55] has a strong influence on the interaction between two adjacent surface atoms and thus affects the electronic structure of surface atoms. If the lattice is compressed, the d-band center will be deeper. If the lattice is expanded, the d-band center will be shallower.[56] Strasser and co-workers investigated the lattice strain effects quantitatively by using dealloyed Pt-based bimetallic catalysts.[5,57,58] The lattice parameter of the Pt–Cu alloy could be tuned by changing the Pt–Cu ratio. Then the level of lattice strain in dealloyed Pt–Cu NCs with Pt–Cu@Pt core–shell structure can be controlled by tuning the core composition. Their work provided a function connecting the ORR activity and the lattice strain in dealloyed Pt–Cu NCs (Fig. 9b).[5]

The barrier for the rate determining step is lowest on the surface with the optimized d-band center position. As for ORR, the main barrier was identified as the structure-sensitive adsorption of OH species and its inhibiting effects on O_2 adsorption. Fig. 9a shows the specific activity towards ORR on different facets of Pt_3Ni and Pt.[54] The Pt_3Ni alloy with the Pt-skin surface shows significantly high activity over Pt, and the specific activities on three low-index facets show an order of Pt_3Ni {100} < Pt_3Ni {110} ≪ Pt_3Ni {111}. Consequently, the Pt–Ni alloy nanooctahedrons with the Pt-skin surface can serve as ORR catalysts with extremely high activity.[8]

Many principle reactions are involved in MOR, and numerous paths might be taken from methanol to CO_2 and H_2O (the final products of MOR). These paths can be generally divided

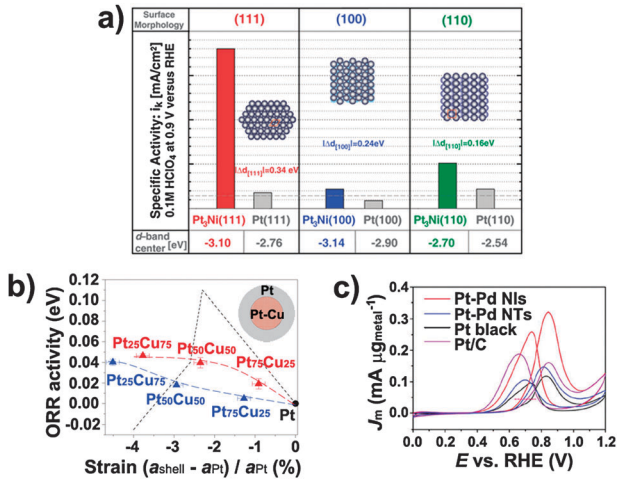

Fig. 9 (a) Specific activity of ORR measured at 0.9 V *versus* RHE on a rotating ring disk electrode in $HClO_4$ (0.1 M) at 333 K with 1600 revolutions per minute on Pt_3Ni {*hkl*} facets as compared to the corresponding Pt {*hkl*} facets (a horizontal dashed gray line marks specific activity of polycrystalline Pt) is shown. Values of the d-band center position obtained from UPS spectra are listed for each facet and compared between corresponding Pt_3Ni {*hkl*} and Pt {*hkl*} facets (modified with permission from ref. 53, copyright 2007 Science). (b) The experimental ORR activity (in units of kT ln(J_{alloy}/J_{Pt}), T = 298 K) of two groups of dealloyed Pt–Cu bimetallic core–shell NCs plotted as a function of lattice strain in the particle shell (red and blue triangles denote dealloyed Pt–Cu bimetallic NCs prepared at an annealing temperature of 800 °C and 950 °C respectively). The inset shows the structure of a dealloyed Pt–Cu bimetallic core–shell NC. The dashed line shows the DFT prediction of the ORR activity for a Pt (111) single-crystalline slab under isotropic strain (modified with permission from ref. 5, copyright 2010 Nature Publishing Group). (c) Cyclic voltammetry (scan rate: 50 mV s^{-1}) curves of different Pt-based catalysts in 0.1 M $HClO_4$ + 1 M CH_3OH solution. The mass activity was normalized in reference to the mass of total metal (modified from ref. 12).

into two classes, the direct path in which CO* is not involved as an intermediate, and the indirect path in which CO* appears as a strong binding intermediate. On the {111} facets of Pt-based alloys, only the direct path is thermodynamically favored at low potentials; the indirect path has a much higher onset potential on that facet. Meanwhile, the onset potential of the {100} facets of the Pt-alloy of both direct and indirect paths is lower than that of the {111} facets. However, CO* poisoning will be much stronger on the {100} facets. Consequently, the durability of the {111} facets is better.[59] In addition, twinned defects in multi-twinned structure NCs can also introduce lattice strain and enhance the cataltic activity of bimetallic NCs. For instance, both Pt–Pd alloy nanoicosahedra (NIs) and nanotetrahedra (NTs) expose {111} facets, while NIs with five-fold twinned defects exhibit higher methanol electrooxidation activity (Fig. 9c).[12]

Unlike low-index facets of bimetallic NCs, atomic steps, terraces and kinks abundantly distribute on high-index facets, where the atomic coordination number is lower (Fig. 1c). These coordinative unsaturated sites are quite active in many catalytic reactions. Therefore, bimetallic NCs exposing high-index facets often show significantly enhanced catalytic performance in many reactions. For instance, Au@Pd NCs exposing high-index facets of Pd show excellent catalytic activity towards Suzuki coupling reaction, which is 3–7 times of that on the {100} facets of Pd.[50]

Increasing the specific surface area (SSA) is another practical idea to increase the mass-specific activity and the utilization rate of noble metals. NCs with hollow or dendritic structures possess high SSA and, unlike ultra small NCs, the high SSA will not decrease obviously due to the aggregation of NCs. A solid core in the dendritic NC can further improve the accessibility of the internal surface of the dendritic shell. For instance, the electrochemically active surface area of Pd–Pt nanodendrites is 57.1 $m^2\ g_{Pt}{}^{-1}$, which is comparable with that of the Pt–C catalyst and far beyond that of Pt black.[16]

4.2 Structural changes of shape-selective bimetallic NCs during catalytic reactions

In general, the structure of metallic NCs tends to evolve into a thermodynamically favored one during catalytic reaction, or even just during aging in solutions.[60–63] Decreasing the total surface free energy is the driving force of these transitions. For instance, Ag[60] and Pd[61] nanocubes would evolve into truncated cubes to expose more {111} facets (which possess lower surface free energy than that of {100} facets) after aging in reaction solutions for a certain time at 160 °C and room temperature, respectively.

In addition to shape changes, metal dissolution and segregation of bimetallic NCs are also involved during catalytic reactions. One example is that the non-noble metal in Pt-based bimetallic NCs tends to be oxidized and dissolved during the electro-catalytic process. The investigation of Carpenter and co-workers showed that Ni atoms in the interior of PtNi alloy NCs tend to be dissolved during the ORR activity testing procedure, and the Pt–Ni framework with a lower Ni–Pt ratio would form after 20k cycles.[39] It is noteworthy that this dissolution process was strongly dependent on the initial composition of the alloy NCs. If the initial content of nickel was 30–36% in a PtNi alloy NC, this NC would be subject to the dissolution of Ni atoms during ORR, while if the initial content of nickel was 40–47%, this NC was more resistant to Ni dissolution. This dissolution procedure can also be utilized to modulate the surface element distribution of bimetallic NCs. For instance, Pt surface-enriched Pt–M (the oxidation potential of M is lower than that of Pt) alloy NCs can be prepared *in situ* by voltammetric dealloying, *i.e.* partial metal dissolution.[62] This method can be used to prepare Pt-skeleton surfaces on Pt–M alloy cores, which showed better ORR activity than Pt–M alloy NCs without dealloying treatment.[53]

Structural changes of bimetallic NCs, especially the segregation process, exist in the heterogeneous catalysis process in gas phase. The driving force of the segregation process is to minimize the total surface energy of bimetallic NCs. For instance, Rh–Pd bimetallic NCs underwent dramatic and reversible structural changes when altering the environment in the sequence of oxidation and reduction.[63] When the NCs were exposed to NO or O_2, Rh would be enriched in the shell, and when they were exposed to the NO–CO mixed environment, Pd would be enriched in the shell. This investigation suggests that the structure of bimetallic NCs under reaction conditions might be totally different from the structure of the ones newly prepared.

5. Conclusions and outlook

Synthesis of bimetallic NCs with well controlled shape has been an important topic in the communities of nanoscience and catalysis. Four general colloidal synthetic routes to prepare bimetallic NCs with well-defined shape are those of continuous growth, crystallites coalescence, seeded growth and galvanic replacement reaction. The reduction potential of metal precursors, interfacial energy, reduction rate, facet-specific capping agents, temperature and reaction time have a strong influence on the structure and shape of bimetallic NCs. Furthermore, the shape of these bimetallic NCs largely impacts their catalytic performance.

Despite these achievements, many significant challenges are still lying in front. From the aspect of synthetic chemistry, general principles and new strategies on surface structure control of bimetallic NCs at the atomic level are of great importance. The shape controlled synthesis of Pt- and Pd-based NCs has been deeply investigated, while in other bimetallic systems, it is still difficult to control the morphology of products. Shape controlled synthesis of Ru- and Rh-based bimetallic NCs might have a great impact. Both as-exploited and new capping agents that can guide the shape evolution in these systems should be further explored, coupled with the molecular-level understanding of the interactions between the functional groups of capping agents and a specific facet based on density functional theory calculations. A more long-range goal is to replace noble metals with non-noble metals, so as to reduce the cost of these nanocatalysts. Since non-noble metals are comparatively difficult to reduce, most commonly used gentle reductants in the aqueous phase are incapable of reducing non-noble metal cations. Thus, the synthetic method in organic solvent, especially the solvothermal method, should be further developed.

From the aspect of catalysis, post-synthesis treatment of bimetallic NCs, especially electro-dissolution and electro-deposition of foreign metal, should also be investigated to enhance the catalytic performance of bimetallic NCs. The influence of capping agents (PVP, fatty acid and fatty amine, halide ions, CO, *etc.*) on catalytic performance of bimetallic NCs remains to be explored. It is necessary to develop methods to remove capping agents from surfaces of bimetallic NCs and simultaneously preserve their structural parameters. Furthermore, how the shapes of bimetallic NCs evolve during the catalytic reaction is still a challenging issue. Operando and *in situ* studies of surface reconstruction and segregation in the catalytic process have recently attracted more and more attention. For instance, ambient-pressure X-ray photoelectron spectroscopy is a strong tool to detect the segregation of surface atoms in alloy NCs exposed to a reactive environment under heating, and environmental transmission electron microscopy can be used to directly observe the shape evolution and facet reconstruction of NCs in time-resolved response to gas and temperature stimuli. Such studies are essential for catching surface chemistry and structure of bimetallic NCs under reaction conditions or during catalysis. With the authentic information of surface structure and chemistry of bimetallic catalysts under reaction conditions, evolution of surface chemistry and morphology during the catalytic process will be revealed. This evolution will guide the synthesis of bimetallic NCs with high activity, selectivity and chemical and thermal stability in return.

Acknowledgements

This work was supported by the NSFC (Grant Nos. 21025101 and 21271011). Y.W.Z. particularly appreciates the financial aid of China National Funds for Distinguished Young Scientists from the NSFC, and the U.S. Department of Energy, Chemical Sciences, Geosciences and Biosciences Division, Office of Basic Energy Sciences, Office of Science, under the grant DE-FG02-12ER1635 and ACS PRF (for F.T. projects at Notre Dame). F.T. acknowledges the financial support from Centre for Sustainable Energy at Notre Dame (c*SEND*). The co-authors also thank Mr Anxiang Yin and Mr Yi Ding for their helpful suggestions and comments in the preparation of this manuscript.

References

1 G. A. Somorjai, *Chem. Rev.*, 1996, **96**, 1223.
2 K. M. Bratlie, H. Lee, K. Komvopoulos, P. Yang and G. A. Somorjai, *Nano Lett.*, 2007, **7**, 3097.
3 T. S. Ahmadi, Z. Wang, T. C. Green, A. Henglein and M. A. El-Sayed, *Science*, 1996, **272**, 1924.
4 M. Chen, D. Kumar, C.-W. Yi and D. W. Goodman, *Science*, 2005, **310**, 291.
5 P. Strasser, S. Koh, T. Anniyev, J. Greeley, K. More, C. Yu, Z. Liu, S. Kaya, D. Nordlund, H. Ogasawara, M. F. Toney and A. Nilsson, *Nat. Chem.*, 2010, **2**, 454.
6 Y. Xia, Y. Xiong, B. Lim and S. E. Skrabalak, *Angew. Chem., Int. Ed.*, 2009, **48**, 60.
7 J. Zhang and J. Fang, *J. Am. Chem. Soc.*, 2009, **131**, 18543.
8 J. Zhang, H. Yang, J. Fang and S. Zou, *Nano Lett.*, 2010, **10**, 638.
9 S. E. Habas, H. Lee, V. Radmilovic, G. A. Somorjai and P. Yang, *Nat. Mater.*, 2007, **6**, 692.
10 J. Wu, A. Gross and H. Yang, *Nano Lett.*, 2011, **11**, 798.
11 A.-X. Yin, X.-Q. Min, Y.-W. Zhang and C.-H. Yan, *J. Am. Chem. Soc.*, 2011, **133**, 3816.
12 A.-X. Yin, X.-Q. Min, W. Zhu, H.-S. Wu, Y.-W. Zhang and C.-H. Yan, *Chem. Commun.*, 2012, **48**, 543.
13 C. Wang, Y. Hou, J. Kim and S. Sun, *Angew. Chem., Int. Ed.*, 2007, **46**, 6333.
14 X. Hong, D. Wang, R. Yu, H. Yan, Y. Sun, L. He, Z. Niu, Q. Peng and Y. Li, *Chem. Commun.*, 2011, **47**, 5160.
15 Z. Peng, H. You and H. Yang, *ACS Nano*, 2010, **4**, 1501.
16 B. Lim, M. Jiang, P. H. C. Camargo, E. C. Cho, J. Tao, X. Lu, Y. Zhu and Y. Xia, *Science*, 2009, **324**, 1302.
17 L. Wang and Y. Yamauchi, *J. Am. Chem. Soc.*, 2010, **132**, 13636.
18 H. Zhang, M. Jin, J. Wang, W. Li, P. H. C. Camargo, M. J. Kim, D. Yang, Z. Xie and Y. Xia, *J. Am. Chem. Soc.*, 2011, **133**, 6078.
19 J. W. Hong, Y. W. Lee, M. Kim, S. W. Kang and S. W. Han, *Chem. Commun.*, 2011, **47**, 2553.
20 H. Zhang, M. Jin, H. Liu, J. Wang, M. J. Kim, D. Yang, Z. Xie, J. Liu and Y. Xia, *ACS Nano*, 2011, **5**, 8212.
21 X. Huang, H. Zhang, C. Guo, Z. Zhou and N. Zheng, *Angew. Chem., Int. Ed.*, 2009, **48**, 4808.
22 H. Zhang, W. Li, M. Jin, J. Zeng, T. Yu, D. Yang, Y. Xia and Y. N. Xia, *Nano Lett.*, 2011, **11**, 898.
23 A.-X. Yin, X.-Q. Min, W. Zhu, W.-C. Liu, Y.-W. Zhang and C.-H. Yan, *Chem.–Eur. J.*, 2012, **18**, 777.
24 E. Bauer and J. H. van der Merwe, *Phys. Rev. B: Condens. Matter Mater. Phys.*, 1986, **33**, 3657.
25 F.-R. Fan, D.-Y. Liu, Y.-F. Wu, S. Duan, Z.-X. Xie, Z.-Y. Jiang and Z.-Q. Tian, *J. Am. Chem. Soc.*, 2008, **130**, 6949.
26 Z. L. Wang, *J. Phys. Chem. B*, 2000, **104**, 1153.
27 E. Herrero, L. J. Buller and H. D. Abruna, *Chem. Rev.*, 2001, **101**, 1897.
28 D. Wang, Q. Peng and Y. Li, *Nano Res.*, 2010, **3**, 574.
29 R. A. Johnson, *Phys. Rev. B: Condens. Matter Mater. Phys.*, 1989, **39**, 12554.
30 H. Zhang, M. Jin, J. Wang, M. J. Kim, D. Yang and Y. Xia, *J. Am. Chem. Soc.*, 2011, **133**, 10422.
31 J. H. Song, F. Kim, D. Kim and P. D. Yang, *Chem.–Eur. J.*, 2005, **11**, 910.
32 M. Jin, H. Zhang, J. Wang, X. Zhong, N. Lu, Z. Li, Z. Xie, M. J. Kim and Y. Xia, *ACS Nano*, 2012, **6**, 2566.
33 H. Lee, S. E. Habas, G. A. Somorjai and P. Yang, *J. Am. Chem. Soc.*, 2008, **130**, 5406.
34 J. W. Hong, D. Kim, Y. W. Lee, M. Kim, S. W. Kang and S. W. Han, *Angew. Chem., Int. Ed.*, 2011, **50**, 8876.
35 Y. W. Lee, M. Kim, S. W. Kang and S. W. Han, *Angew. Chem., Int. Ed.*, 2011, **50**, 3466.
36 Y. W. Lee, M. Kim, Y. Kim, S. W. Kang, J.-H. Lee and S. W. Han, *J. Phys. Chem. C*, 2010, **114**, 7689.
37 J. Wu and H. Yang, *Nano Res.*, 2011, **4**, 72.
38 Y. Wu, S. Cai, D. Wang, W. He and Y. Li, *J. Am. Chem. Soc.*, 2012, **134**, 8975.
39 M. K. Carpenter, T. E. Moylan, R. S. Kukreja, M. H. Atwan and M. M. Tessema, *J. Am. Chem. Soc.*, 2012, **134**, 8535.
40 D. Xu, Z. Liu, H. Yang, Q. Liu, J. Zhang, J. Fang, S. Zou and K. Sun, *Angew. Chem., Int. Ed.*, 2009, **48**, 4217.
41 C.-L. Lu, K. S. Prasad, H.-L. Wu, J.-a. A. Ho and M. H. Huang, *J. Am. Chem. Soc.*, 2010, **132**, 14546.
42 C.-W. Yang, K. Chanda, P.-H. Lin, Y.-N. Wang, C.-W. Liao and M. H. Huang, *J. Am. Chem. Soc.*, 2011, **133**, 19993.
43 V. K. LaMer and R. H. Dinegar, *J. Am. Chem. Soc.*, 1950, **72**, 4847.
44 Q. Liu, Z. Yan, N. L. Henderson, J. C. Bauer, D. W. Goodman, J. D. Batteas and R. E. Schaak, *J. Am. Chem. Soc.*, 2009, **131**, 5720.
45 L. Wang and Y. Yamauchi, *Chem.–Asian J.*, 2010, **5**, 2493.
46 L. Zhang, J. Zhang, Q. Kuang, S. Xie, Z. Jiang, Z. Xie and L. Zheng, *J. Am. Chem. Soc.*, 2011, **133**, 17114.
47 F. Wang, L.-D. Sun, W. Feng, H. Chen, M. H. Yeung, J. Wang and C.-H. Yan, *Small*, 2010, **6**, 2566.
48 M. Jiang, B. Lim, J. Tao, P. H. C. Camargo, C. Ma, Y. Zhu and Y. Xia, *Nanoscale*, 2010, **2**, 2406.
49 H. Kobayashi, B. Lim, J. Wang, P. H. C. Camargo, T. K. Yu, M. J. Kim and Y. Xia, *Chem. Phys. Lett.*, 2010, **494**, 249.
50 F. Wang, C. Li, L.-D. Sun, H. Wu, T. Ming, J. Wang, J. C. Yu and C.-H. Yan, *J. Am. Chem. Soc.*, 2011, **133**, 1106.

51 D. Kim, Y. W. Lee, S. B. Lee and S. W. Han, *Angew. Chem., Int. Ed.*, 2012, **51**, 159.
52 H. Liu, J. Qu, Y. Chen, J. Li, F. Ye, J. Y. Lee and J. Yang, *J. Am. Chem. Soc.*, 2012, **134**, 11602.
53 V. R. Stamenkovic, B. S. Mun, M. Arenz, K. J. J. Mayrhofer, C. A. Lucas, G. Wang, P. N. Ross and N. M. Markovic, *Nat. Mater.*, 2007, **6**, 241.
54 V. R. Stamenkovic, B. Fowler, B. S. Mun, G. Wang, P. N. Ross, C. A. Lucas and N. M. Markovic, *Science*, 2007, **315**, 493.
55 A. U. Nilekar, S. Alayoglu, B. Eichhorn and M. Mavrikakis, *J. Am. Chem. Soc.*, 2010, **132**, 7418.
56 R. R. Adzic, J. Zhang, K. Sasaki, M. B. Vukmirovic, M. Shao, J. X. Wang, A. U. Nilekar, M. Mavrikakis, J. A. Valerio and F. Uribe, *Top. Catal.*, 2007, **46**, 249.
57 P. Strasser, *Rev. Chem. Eng.*, 2009, **25**, 255.
58 M. Oezaslan, M. Heggen and P. Strasser, *J. Am. Chem. Soc.*, 2012, **134**, 514.
59 P. Ferrin and M. Mavrikakis, *J. Am. Chem. Soc.*, 2009, **131**, 14381.
60 J. Chen, J. M. McLellan, A. Siekkinen, Y. Xiong, Z. Li and Y. Xia, *J. Am. Chem. Soc.*, 2006, **128**, 14776.
61 Y. Xiong, H. Cai, B. J. Wiley, J. Wang, M. J. Kim and Y. Xia, *J. Am. Chem. Soc.*, 2007, **129**, 3665.
62 S. Koh and P. Strasser, *J. Am. Chem. Soc.*, 2007, **129**, 12624.
63 F. Tao, M. E. Grass, Y. Zhang, D. R. Butcher, J. R. Renzas, Z. Liu, J. Y. Chung, B. S. Mun, M. Salmeron and G. A. Somorjai, *Science*, 2008, **322**, 932.